Theor Chem Acc (2014) 133:1551
DOI 10.1007/s00214-014-1551-0

REGULAR ARTICLE

First-principles investigations on the anisotropic charge transport in 4,4′-bis((*E*)-2-(naphthalen-2-yl)vinyl)-1,1′-biphenyl single crystal

Lili Lin · Xin Li · Guangjun Tian · Hua Geng · Zhigang Shuai · Yi Luo

Received: 30 June 2014 / Accepted: 19 July 2014 / Published online: 6 August 2014

Abstract We applied the master equation method to investigate the anisotropic transport property of the 4,4′-bis((*E*)-2-(naphthalen-2-yl)vinyl)-1,1′-biphenyl molecular crystal based on first-principles calculation. It is found that the hole mobility has the largest value along the [100] direction, while electrons have the best transport property along the [010] direction. The anisotropic transport property was found to have close relationship with the charge transfer integral which is determined by the molecular stacking network in the crystals as well as the intermolecular frontier orbital overlap. In addition, the effect of the charge carrier density and the electronic field on the charge transport was also studied, and little effect was found except that the density is larger than 0.01 and the electronic field is increased to 1.0×10^6 V/cm. The kinetic Monte Carlo simulation method has also been used to study the anisotropic charge transport property, and consistent results were obtained as with the master equation method.

Keywords Organic electronics · Carrier mobility · Charge transfer · Master equation · Crystal anisotropy

1 Introduction

Organic molecular crystals, as one of the most important components in organic solar cells, organic field-effect transistors, and organic light-emitting diodes, have attracted much attention of both theoretical and experimental researchers, and many excellent molecular crystals have been designed and integrated into functional devices [1–3]. Since the charge transport is an essential process in all these devices, its mechanism has become an enthusiastically controversial topic regarding both electrical and optical measurements [4–6] and some general rules have been proposed [7, 8]. To better understand the transport mechanism, it is desirable to gain knowledge of the anisotropic transport property of organic molecular crystals which is closely related to the stacking configurations and the molecular structures. To date, the anisotropy of transport property has been investigated only in a few molecular crystals, such as rubrene (5,6,11,12-tetraphenyltetracene), CH4T(dicyclohexyl-α-quaterthiophene), pentacene, and tetracene, all of which are studied on the two-dimensional (2-D) charge transport [9–14]. Recently, Tao group for the first time performed the measurement of the three-dimensional (3-D) charge transport in the 4,4′-bis((*E*)-2-(naphthalen-2-yl)vinyl)-1,1′-biphenyl (BNVBP) molecular

Dedicated to Professor Guosen Yan and published as part of the special collection of articles celebrating his 85th birthday.

L. Lin
College of Physics and Electronics, Shandong Normal University, Jinan 250014, China

L. Lin · X. Li · G. Tian · Y. Luo
Department of Theoretical Chemistry and Biology, School of Biotechnology, Royal Institute of Technology, 10691 Stockholm, Sweden

H. Geng
Key Laboratory of Organic Solids, Beijing National Laboratory for Molecular Sciences (BNLMS), Institute of Chemistry, Chinese Academy of Sciences, Beijing 100190, China

Z. Shuai (✉)
Department of Chemistry, Tsinghua University, Beijing 100084, China
e-mail: zgshuai@tsinghua.edu.cn

Y. Luo
Hefei National Laboratory for Physical Sciences at the Microscale, University of Science and Technology of China, Hefei 230026, Anhui, China

crystal with two kinds of morphology and orientation and the highest hole mobility was found along the *a*-axis direction [15]. In this work, we apply the master equation (ME) method to investigate the anisotropic property of the charge carrier mobility based on the first-principles calculations. The calculated results are found in good agreement with the experiment. The influence of the electric field and the carrier density on mobility has also been studied. The 3-D transport property of the intrinsic diffusion mobility was also investigated based on the kinetic Monte Carlo (MC) simulations, and the similar anisotropic property was found. The theoretical investigation helps for better understanding of the transport mechanism and intrinsic property of the BNVBP molecular crystal.

2 Methodology

In this paper, both the drift mobility and the diffusion mobility are investigated. For the drift mobility, the incoherent motion of the carriers is described by the Pauli Master equation [16]:

$$\frac{\partial \rho_i}{\partial t} = -\sum_{j\neq i}\left[W_{ji}\rho_i(1-\rho_j) - W_{ij}\rho_j(1-\rho_i)\right] \tag{1}$$

Here, ρ_i is the charge carries population density of site i and the $(1-\rho_j)$ represents the Coulomb penalty of site j due to the occupation of charge carriers. W_{ji} is defined as the charge carrier transition rate from site i to site j, and it can be calculated using the Marcus–Hush electron transfer theory at the high-temperature limit [17, 18]:

$$W_{ji} = \frac{V_{ji}^2}{\hbar}\sqrt{\frac{\pi}{K_B T\lambda}}\cdot\exp\left[-\frac{\left(\mp\Delta G_{ji}+\lambda\right)^2}{4\lambda K_B T}\right] \tag{2}$$

Here, V_{ji} is the transfer integral between site i and site j, and λ is the reorganization energy. ΔG_{ji} is the site energy difference between the site i and site j, and it is defined as

$$\Delta G_{ji} = E_j - E_i \tag{3}$$

where E_i is the free energy of site i. The sign of minus before the site energy difference in Eq. (2) is adopted for holes, and the positive sign is used for the electrons. When an electric field is applied, the site energy is modulated as

$$\Delta G_{ji} = E_j - E_i + |e|\vec{F}\cdot\vec{R}_{ji} \tag{4}$$

where $\vec{F}$ is the electronic field and $\vec{R}_{ji}$ is the displacement between site i and site j:

$$\vec{R}_{ji} = \vec{R}_j - \vec{R}_i. \tag{5}$$

As the measurement is performed at the steady state, the charge carrier population is assumed to be constant. The steady master equation is expressed as follows:

$$0 = -\sum_{j\neq i}\left[W_{ji}\rho_i(1-\rho_j) - W_{ij}\rho_j(1-\rho_i)\right] \tag{6}$$

The charge carrier population at the steady state can be calculated by the iterative procedure:

$$\rho_i = \frac{\sum_j W_{ij}\rho_j}{\sum_j W_{ji} + \sum_j\left(W_{ij}-W_{ji}\right)\rho_j} \tag{7}$$

Then, the charge carrier mobility can be calculated:

$$\mu = \frac{\sum_{i,j} W_{ji}\rho_i(1-\rho_j)\widehat{F}\cdot\vec{R}_{ji}}{\rho_{\text{tot}}|F|} \tag{8}$$

Here, $\widehat{F}$ is the unit vector of the electric field, and ρ_{tot} is the total charge carrier population in the investigated supercell. In this paper, the 5 × 5 × 5 supercell is large enough to give the consistent result and periodic boundary condition has also been applied. Based on these equations, we can also investigate the influence of the charge carrier density and the electric field.

When there is no electric field, the charge carriers can also diffuse in the molecular crystals, and the intrinsic charge mobility can be calculated using the Einstein equation

$$\mu = \frac{eD}{K_B T} \tag{9}$$

where D is the diffusion coefficient, and it can obtained by performing the kinetic Monte Carlo simulation. In the simulation, the crystal structure is used and one charge is only allowed to transport to neighbor molecules with the probability as $P_{ki} = \frac{W_{ki}}{\sum_j W_{kj}}$. The sum runs over all the possible paths when one charge is located at site k. At each step, one random number r is generated. If the number r satisfies $\sum_{i=1}^{\alpha-1} P_{ki} < r \leq \sum_{i=1}^{\alpha} P_{ki}$, then the charge will transport through the α path. For the detailed simulation method, one can refer to the Ref. [19]. By repeating the process for thousands times, the averaged value with respect to the time follows a linear relationship. The ratio is the diffusion coefficient according to

$$D = \lim_{t\to\infty}\frac{r^2}{2nt} \tag{10}$$

where r and t are the averaged displacement and total time span. Here, n represents the dimension of the charge transport in the crystal. In our calculation, the 10 × 10 × 3 supercell is adopted. The time limit for each simulation was set as 0.01 ns and 2,000 trajectories were chosen to get the average value of the diffusion coefficient D.

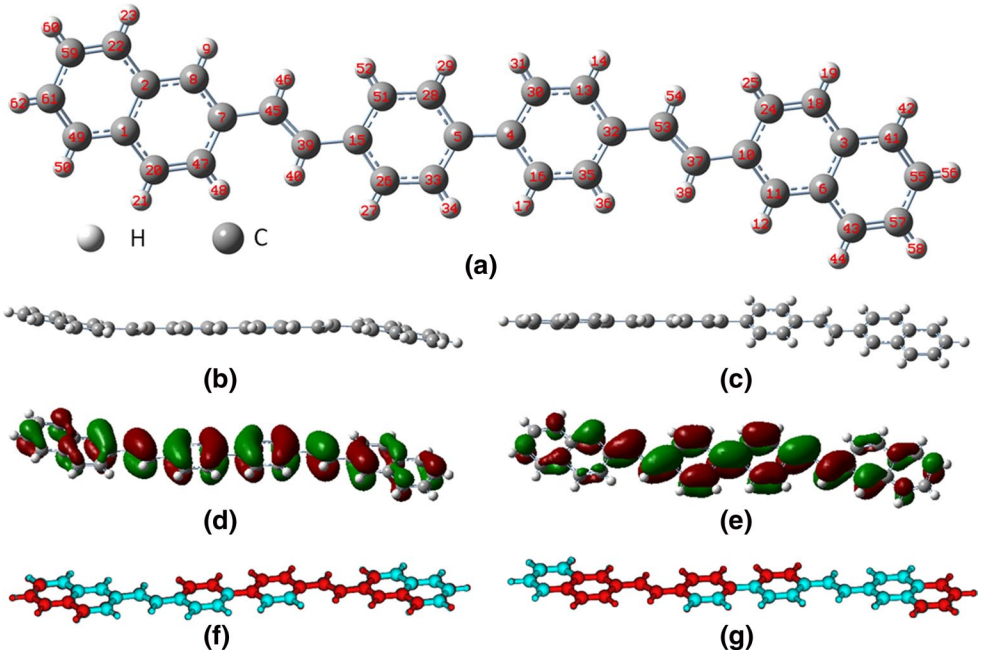

Fig. 1 **a** The structure and atom labels of the BNVBP molecule, **b** and **c** are the structure of the BNVBP molecule in the crystal and the gas phase separately, **d** and **e** show the electron distribution of the HOMO and LUMO, respectively, **f** shows the overlayer structure of the optimized neutral (*cyan*) and cation (*red*) molecule, and **g** is the overlayer structure of the neutral (*cyan*) and anion (*red*) molecule

In this work, the charge carrier transition rate is calculated using the Marcus rate equation where the transfer integral and the reorganization energy are two important parameters. Lots of methods have been developed to calculate the transfer integral [20–26], and here, the site energy correction method is adopted [23–25]. The reorganization energy is calculated using the adiabatic potential energy surface method (AP) [23]. The normal mode analysis method (NM) [27] has also been used for validation [28]. The calculation of the transfer integral is based on the electronic structure calculation using the PW91PW91/6-31g* method. To calculate the reorganization energy, the geometry of the molecule is first optimized and then, the frequency and electronic structure calculation are performed using the B3LYP/6-31g* method. All the quantum chemistry calculation is realized in the Gaussian 09 program [29].

Table 1 Structure parameters of the BNVBP molecule in the crystal and gas phase. The numbers shown in the first column are the atom numbers shown in Fig. 1a (unit: degree)

Angles	Crystal	Gas	Difference
47-7-45-39	−9.337	1.087	10.424
53-37-10-24	11.295	0.189	11.106
45-39-15-51	4.039	1.637	2.402
13-32-53-37	175.110	179.860	4.750
28-5-4-30	0.051	34.682	34.631
47-7-45	121.647	123.043	1.396
45-39-15	128.324	127.111	1.213
39-15-51	124.696	123.968	0.728
28-5-4	121.935	121.287	0.648
13-32-53	118.421	118.969	0.548
53-37-10	125.405	127.120	1.715
37-10-11	119.293	119.049	0.244

3 Results and discussion

3.1 Geometric comparison

To calculate the reorganization energy, the BNVBP molecule (see Fig. 1a) was first optimized in the gas phase. Compared with the structure in the crystal, the most significant difference lies in the dihedral angle between the two phenyls at the center of the molecule (see Fig. 1b, c). In the crystal structure, the two phenyl rings in the center are at the same surface, so are the C=C double bonds. However, significant dihedral angle (about 34.68°) can be found between the two phenyl rings in the center of the molecule in gas phase. From Fig. 1b, c, we can also see that the dihedral angles between the end naphthalene groups and the central part also differ with each other. In the crystal structure, the naphthalene groups at two ends outstand the central surface and the angles are as large as 10.42° and 11.10°, respectively; however, they keep the same surface with the phenyl rings connected by the C=C double bond at each side in gas phase. Other significant differences between the structures in crystal and gas phase are listed in Table 1. We can see that the differences mainly arise from the dihedral angles and the angles between bonds. The bond length involved in this molecule has little difference (no more than 0.1 Å) between the crystal and gas structures which is therefore not listed here.

Table 2 Reorganization energy of electrons and holes calculated using the AP method and NM method (unit: meV)

Method	Electron	Hole
AP	215	175
NM	215	175

3.2 Electronic structure

Based on the electronic structure calculations of the BNVBP molecule in crystal structure, the highest occupied molecular orbital (HOMO) and the lowest unoccupied molecular orbital (LUMO) are shown in Fig. 1d, e. Clearly, both the HOMO and LUMO are delocalized orbitals; thus, similar transfer integrals are expected both for holes and electrons. The calculated energy for HOMO is −5.14 eV which is close to the work function of gold (5.1 eV). The energy for LUMO is −1.81 eV which does not match with the metal electrode and is easy to be ionized in the air. Consequently, BNVBP should be used as a p-type semiconductor material.

3.3 Reorganization energy

To simulate the property of BNVBP molecules in crystals, the dihedral angle 28-5-4-30 is frozen during the calculation of the reorganization energy. Two kinds of methods have been employed to calculate the reorganization energy, namely the AP method and NM method. It is shown in Table 2 that the reorganization energy calculated with the NM method is fully consistent with the AP method. As illustrated in this table, holes have smaller reorganization energy than electrons and larger mobility is expected for holes. The comparison between the structures of the cation and the neutral state is shown in Fig. 1f. These two structures have very good overlap, and no significant difference can be found, which reflects small reorganization energy induced when one electron is withdrawn from the molecule. The similar phenomenon can also be found for the anion and neutral states (see Fig. 1g).

The reorganization energy of holes contributed by every vibration modes can also be obtained with the NM method, as illustrated in Fig. 2. It is found that the profiles for the neutral state and the cation state are quite similar. Most of the vibration modes have little contribution to the reorganization energy. The main contribution comes from the C=C stretching vibration modes in the biphenyl of the molecule and the C=C bonds. The stretching mode of the two naphthalene groups in the molecule and the C–H in-plane bending modes have also significant contributions. The reorganization energy for anions contributed by vibration modes has also been calculated, and similar profile is obtained as that for holes.

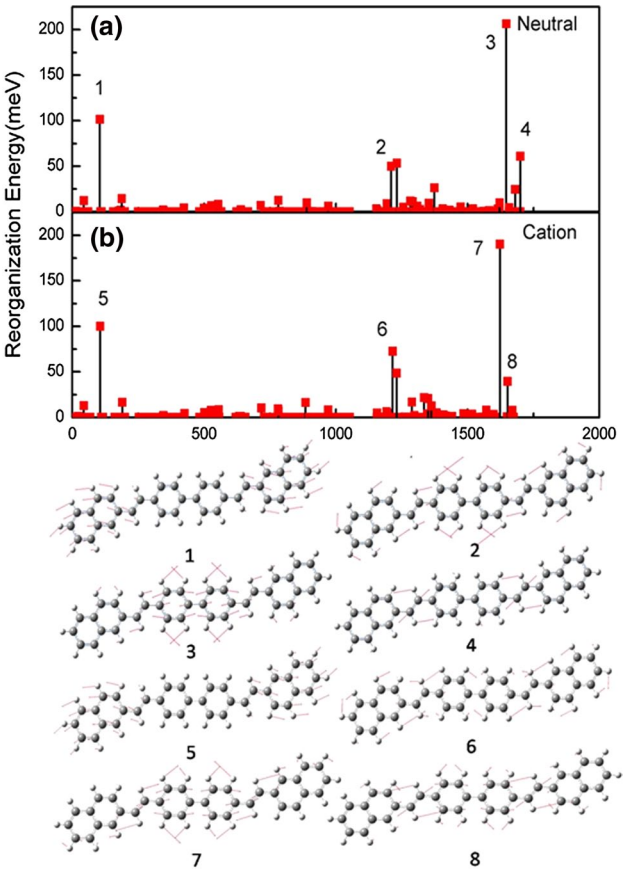

Fig. 2 Reorganization energy contributed by vibration modes of neutral state (**a**) and cation state (**b**). The vibration profiles of vibration modes with significant contribution to the reorganization energy are shown at the *bottom* of the figure

3.4 Transfer integral

Another important factor that determines the charge carrier mobility is the intermolecular transfer integral which depends on both the molecule geometry and the stacking structure. The unit cell of the BNVBP molecular crystal is shown in Fig. 3a, where the crystal structure comes from Ref. [12]. One can see that molecule arranged in a herringbone pattern. The main transfer paths on the (001) and (010) surface are illustrated in Fig. 3b, c. The transfer integral of holes and the intermolecular distances are listed in Table 3. It can be seen that the transfer integrals along the six different paths on the (001) surface are much larger than those on the (010) surface. The large separation between the molecules along the paths on (010) surface makes the transfer integral very small. It has been widely accepted that larger transfer integral can be generated along π stacking directions. In this study, the intermolecular distance along the π stacking direction is larger than the other directions on the (001) surface; thus, smaller transfer integral is obtained. Correspondingly, the transfer integral of electrons is also shown in Table 3. One can see that

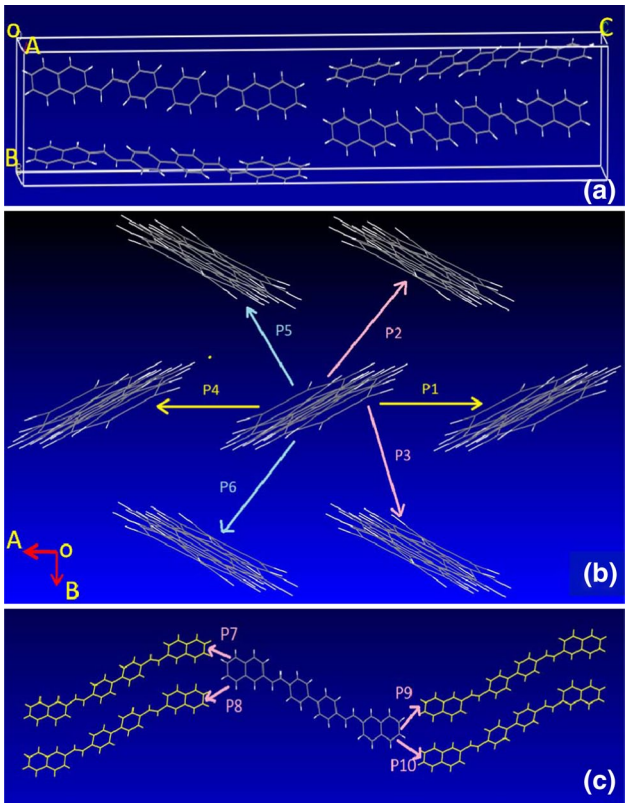

Fig. 3 **a** The unit cell of the BNVBP molecular crystal detected in experiment, **b** and **c** present the transfer paths on the (001) surface and the (010) surface

the transfer integrals along the paths on the (010) surface are quite small as well. The transfer integrals along the π stacking direction become much smaller than those along the other four paths on the (001) surface, which implies lower electron mobility along the π stacking direction.

3.5 Electric field and charge carrier density dependences of drift mobility

Based on the above calculations, one can find that the transfer integral is much smaller than the reorganization energy for both holes and electrons, which implies that charge carriers transport by hopping between molecules. The hopping rate can be calculated according to the Marcus rate equation; consequently, the drift mobility can be obtained by solving the master equations. In the calculations of the drift mobility, two parameters need to be determined. One is the charge carrier density; the other is the magnitude of the electronic field. In the experiment, the applied voltage is 80 V and the length of the OFET is about 7.3 μm [15]. The electric field is about $F = V/L = 1.0 \times 10^5$ V/cm. The charge carrier density is determined by gate voltage, difficult to be measured in experiment. Nevertheless, the influence of the charge carrier density on the drift mobility can be simulated in our theoretical method (see Fig. 4a). Here, the electric field is assumed to be 1.0×10^5 V/cm, and the voltage is applied along the [100] direction. It is illustrated that there is no significant influence on the mobility when the charge carrier density is small. When the carrier density is larger than 0.01, the mobility decreases significantly with the increase in the carrier density. This is due to less available sites left for charge to transport in the molecular crystal; consequently, charge transport will be hindered.

The influence of the electric field on the drift mobility is quite complicated (see Fig. 4b). When the electronic field is in the range of 10^2–10^6 V/cm, the drift mobility has no significant change. When the electric field is larger than 1.0×10^6 V/cm, the drift mobility increases at first and then decreases. This happens when the inverted regime of Marcus theory is approached (i.e., at the semiclassical level, when $\Delta G_{ji} > \lambda$). In that regime, the increase in driving force will lead to a reduction in transfer rate and hence in mobility. It should be noted that the charge carrier density of 0.001 is adopted. Similar properties can be found for electrons. It is found that the drift mobility for electrons is about half of the values of holes. In addition, one can find that the turning point of the electronic field for electrons is at 5.04×10^6 V/cm, but at 2.01×10^6 V/cm for holes. From Eqs. (2) and (4), one can conclude that the difference

Table 3 Transfer integrals of holes and electrons along different paths in molecular crystals

Transfer paths	Central distances (Å)	Transfer integral of holes (meV)	Transfer integral of electrons (meV)
P1	5.97	−17.41	9.26
P2	4.80	22.24	−30.87
P3	4.80	22.24	−30.87
P4	5.97	−17.41	9.26
P5	4.80	19.91	−29.67
P6	4.80	19.91	−29.67
P7	26.95	0.012	0.014
P8	26.90	0.347	−0.427
P9	26.95	0.015	0.038
P10	26.90	0.350	−0.421

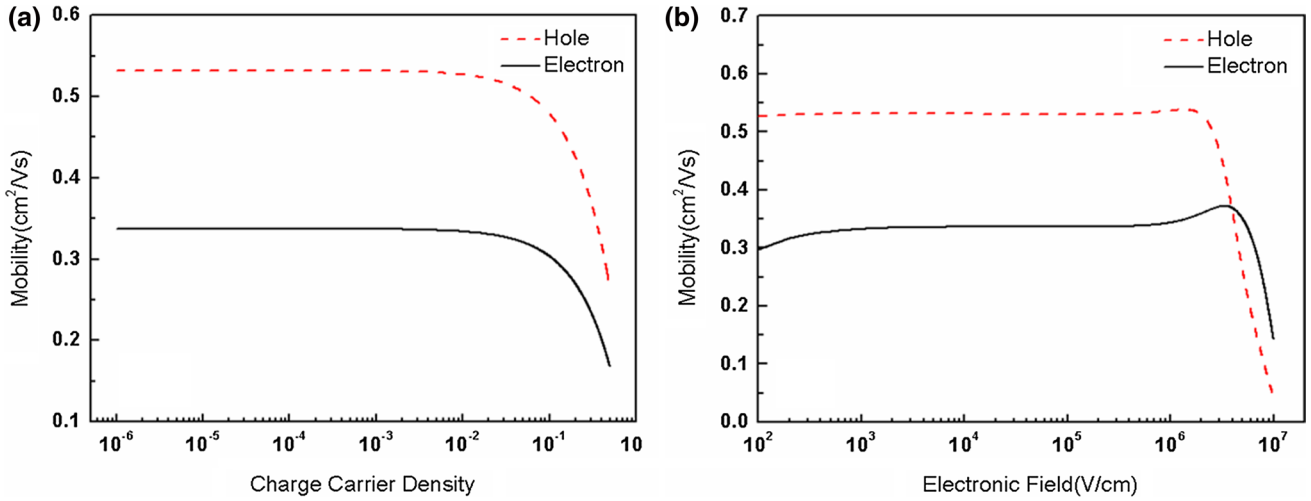

Fig. 4 **a** Charge carrier density dependence of the hole mobility (*dashed line*) and electron mobility (*solid line*), **b** electronic field dependence of hole mobility and electron mobility

mainly arises from the deviation of the reorganization energy of electrons and holes.

3.6 Anisotropic property

In the study of the anisotropic property of the drift mobility, the electric field is fixed as 1.0×10^5 V/cm and the charge carrier density of 0.001 is adopted. The anisotropic properties of the holes as well as the electrons calculated with both ME and MC methods are shown in Fig. 5. The angles on the (001), (100), and (010) surface in Fig. 5 are defined as the angles between the electric field and the OA ([100]), OB ([010]), and OC ([001]) directions, respectively. It is clear that the mobility calculated with ME method has the same anisotropic property as the diffusion mobility calculated with the MC method for both holes and electrons. Considering the computational errors, the mobility calculated with both methods is in good agreement with each other. As illustrated in Fig. 5a, the holes have larger mobility along the [100] direction than that along the [010] direction. The hole mobility along the [001] direction is much smaller than that along the [010] direction (see Fig. 5b) and the [100] direction (see Fig. 5c). It is concluded that holes have the largest mobility along the [100] direction. This is understandable if we analyze the result of the transfer integrals. From Table 3 and Fig. 3b, we can see that not only the transfer integrals of holes along P1 and P4, but also that along P2, P3, and P4 and P5 will have large contribution to the charge transport along the [100] direction, although the transfer integral along P1 and P4 is smaller than that along the other four paths. However, charge transport along [010] direction is only determined by the transfer integral along P3, P4, P5, and P6. From Fig. 5d, we find that the electrons have the largest mobility along the [010] direction, which is different from that of holes. Similarly, the reason mainly arises from the difference of the transfer integral. One can see that the transfer integral of electrons along the π stacking direction ([100]) is much smaller compared with that of holes, while the transfer integrals along other paths are relatively large which will induce large electron mobility on the [010] direction. The electron mobility on the [001] direction is also the smaller than that along [100] direction (see Fig. 5f), which is in consistent with that of holes. Our theoretical investigation shows the close relationship between the anisotropic property of the mobility and the transfer integrals.

The mobility of holes and electrons calculated with both ME and MC methods along [100], [010], and [001] directions is listed in Table 4. The anisotropic property of the hole mobility is [100] > [010] > [001]; however, for electrons, it is [010] > [100] > [001]. It is clear that the electron mobility along [100] direction is about one half of the hole mobility, while the electron mobility along the [010] direction is almost the same as the hole mobility. It can also be seen that the hole mobility along the [100] direction is 0.532 cm^2/Vs, which is a little smaller than the experimental value (2.3 ± 0.2 cm^2/Vs) measured on the plate-shaped single-crystal OFETs but almost the same as the value (0.40 ± 0.25 cm^2/Vs) measured on the rod-shaped single-crystal OFETs [15]. The calculated hole mobility along [100] direction is about one and half times as large as that along the [010] direction, which is in consistent with the experimental result. From the anisotropic property on the (001) surface, we can deduce that the hole mobility along [110] direction should be in the middle of the value along [100] direction and [010] direction. However,

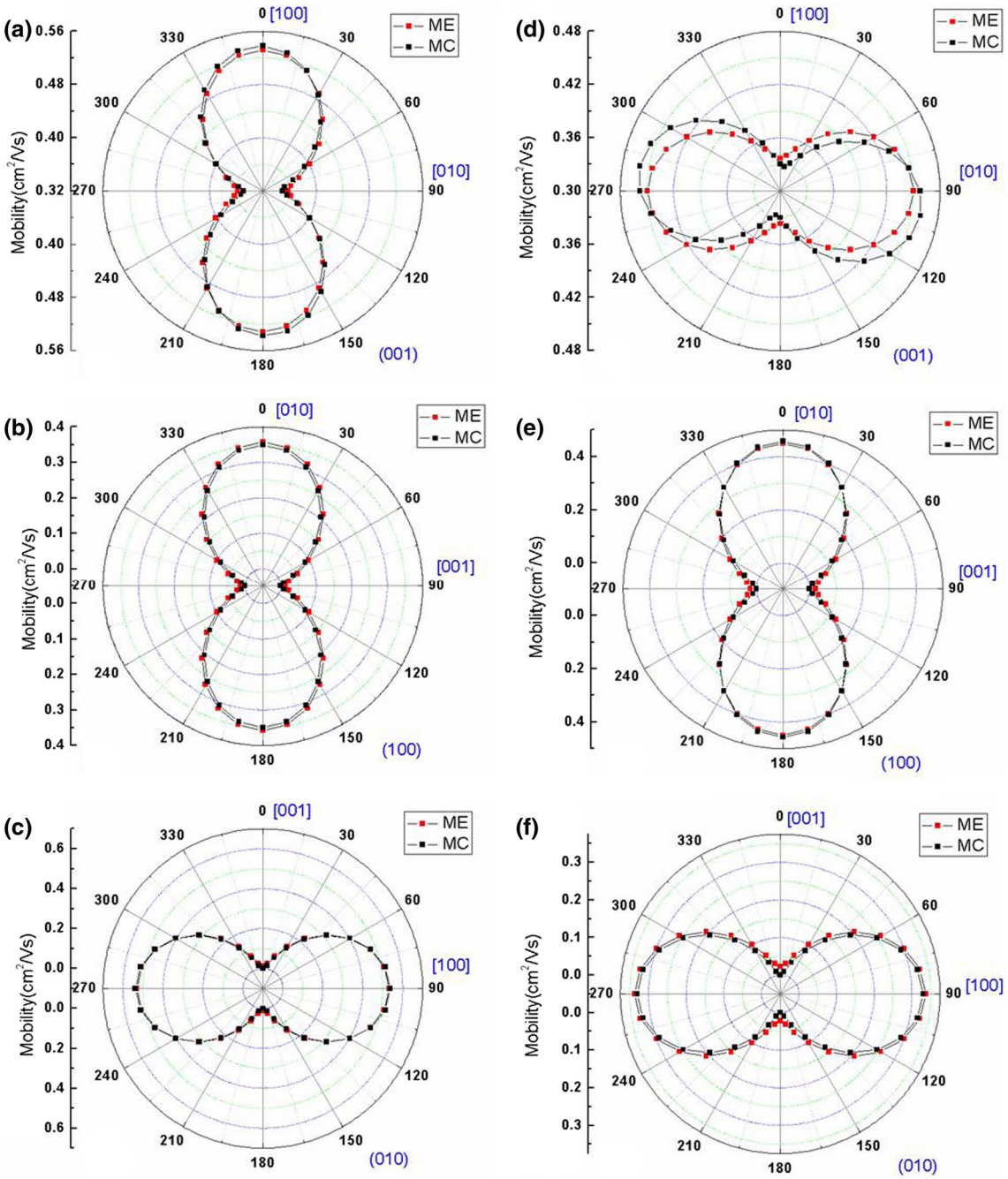

Fig. 5 **a–c** Hole mobility on the (001), (100), and (010) surface, **d–f** electron mobility on the (001), (100), and the (010) surface

Table 4 Mobility of holes and electrons along different directions calculated with both ME and MC methods and the averaged diffusion mobility (unit: cm^2/Vs)

Methods	ME			MC			
Direction	[100]	[010]	[001]	[100]	[010]	[001]	Average
Hole	0.532	0.358	0.013	0.538	0.349	0.000	0.444
Electron	0.337	0.450	0.020	0.330	0.458	0.000	0.394

the experimental measurement shows that the hole mobility along [110] direction is smaller than that along the [010] direction. This discrepancy may be induced by many factors, such as the defect, traps, grain boundaries, and so on.

4 Conclusion

In summary, the anisotropic property of the hole mobility and electron mobility of the BNVBP molecular crystal were investigated with both ME and MC methods. The charge carrier mobility values calculated with two methods are consistent with each other. The anisotropic property of electron mobility on the (001) surface is different from that of hole mobility, due to difference in intermolecular frontier orbital overlap: HOMO for hole and LUMO for electron. The BNVBP molecular crystal has the largest hole mobility on the [100] direction, while the best transport direction for electrons is along the [010] direction. The relationship between the anisotropic property of mobility and transfer integral has been established. Our calculation confirms that the BNVBP molecular crystal has better transport property as p-type materials than the n-type materials. The study indicates that the charge carrier density and the electronic field have little effect on the drift mobility except that the density is larger than 0.01 and the electronic field is increased to 1.0×10^6 V/cm. It should be noted that the basic assumption here is the localized charge hopping model, which is in qualitative agreement with the experiment. More general considerations should include charge delocalization effect, quantum nuclear tunneling, as well as non-perturbative charge dynamics, which deserve further investigations [30].

Acknowledgments This work is supported by the National Natural Science Foundation of China (Grant Nos. 21290191, 11247307, 11304172, and 91333202) and the Ministry of Science and Technology through 973 program (Grant Nos. 2010CB923300, 2011CB932304, 2011CB808405, 2013CB933503), and the Göran Gustafsson Foundation for Research in Natural Sciences and Medicine. The Swedish National Infrastructure for Computing (SNIC) is acknowledged for computational time. Great thanks to Professor Shiwei Yin, Dr Weijie Hua, and Dr. Sai Duan for helpful discussion.

References

1. Lin Y, Li Y, Zhan X (2012) Small molecule semiconductors for high-efficiency organic photovoltaics. Chem Soc Rev 41(11):4245
2. Meng Q, Hu W (2012) Recent progress of n-type organic semiconducting small molecules for organic field-effect transistors. Phys Chem Chem Phys 14(41):14152
3. Wang C, Dong H, Hu W, Liu Y, Zhu D (2012) Semiconducting π-conjugated systems in field-effect transistors: a material odyssey of organic electronics. Chem Rev 112(4):2208–2267
4. Sakanoue T, Sirringhaus H (2010) Band-like temperature dependence of mobility in a solution-processed organic semiconductors. Nat Mater 9:736–740
5. Geng H, Peng Q, Wang LJ, Li HJ, Liao Y, Ma ZY, Shuai Z (2012) Toward quantitative prediction of charge mobility in organic semiconductors: tunneling enabled hopping model. Adv Mater 24:3568–3572
6. Jiang YQ, Xu HH, Zhao N, Peng Q, Shuai Z (2014) Spectral signature of intrachain and interchain polarons in donor-acceptor copolymers. Acta Chim Sinica 72(2):201–207
7. Shuai Z, Wang L, Li Q (2011) Evaluation of charge mobility in organic materials: from localized to delocalized descriptions at a first-principles level. Adv Mater 23(9):1145–1153
8. Troisi A (2011) Charge transport in high mobility molecular semiconductors: classical models and new theories. Chem Soc Rev 40(5):2347–2358
9. Sundar VC, Zaumseil J, Podzorov V, Menard E, Willett RL, Someya T, Gershenson ME, Rogers JA (2004) Elastomeric transistor stamps: reversible probing of charge transport in organic crystals. Science 303(5664):1644–1646
10. Zeis R, Besnard C, Siegrist T, Schlockermann C, Chi X, Kloc C (2006) Field effect studies on rubrene and impurities of rubrene. Chem Mater 18(2):244–248
11. Lee JY, Roth S, Park YW (2006) Anisotropic field effect mobility in single crystal pentacene. Appl Phys Lett 88(25):252106–252106–3
12. Mannsfeld SCB, Locklin J, Reese C, Roberts ME, Lovinger AJ, Bao Z (2007) Probing the anisotropic field-effect mobility of solution-deposited dicyclohexyl-α-quaterthiophene single crystals. Adv Funct Mater 17(10):1617–1622
13. Reese C, Bao Z (2007) High-resolution measurement of the anisotropy of charge transport in single crystals. Adv Mater 19(24):4535–4538
14. Xia Y, Kalihari V, Frisbie CD, Oh NK, Rogers JA (2007) Tetracene air-gap single-crystal field-effect transistors. Appl Phys Lett 90(16):162106–162106
15. He T, Zhang X, Jia J, Li Y, Tao X (2012) Three-dimensional charge transport in organic semiconductor single crystals. Adv Mater 24(16):2171–2175
16. Pasveer WF, Cottaar J, Tanase C, Coehoorn R, Bobbert PA, Blom PWM, de Leeuw DM, Michels MAJ (2005) Unified description of charge-carrier mobilities in disordered semiconducting polymers. Phys Rev Lett 94(20):206601
17. Hush NS (1968) Homogeneous and heterogeneous optical and thermal electron transfer. Electrochim Acta 13(5):1005–1023
18. Marcus RA (1993) Electron transfer reactions in chemistry. Theory and experiment. Rev Mod Phys 65(3):599–610
19. Wang L, Nan G, Yang X, Peng Q, Li Q, Shuai Z (2010) Computational methods for design of organic materials with high charge mobility. Chem Soc Rev 39(2):423–434
20. Paulson BP, Curtiss LA, Bal B, Closs GL, Miller JR (1996) Investigation of through-bond coupling dependence on spacer structure. J Am Chem Soc 118(2):378–387
21. Grozema FC, van Duijnen PT, Berlin YA, Ratner MA, Siebbeles LDA (2002) Intramolecular charge transport along isolated chains of conjugated polymers: effect of torsional disorder and polymerization defects. J Phys Chem B 106(32):7791–7795
22. Senthilkumar K, Grozema FC, Bickelhaupt FM, Siebbeles LDA (2003) Charge transport in columnar stacked triphenylenes: effects of conformational fluctuations on charge transfer integrals and site energies. J Chem Phys 119(18):9809–9817
23. Lemaur V, da Silva Filho DA, Coropceanu V, Lehmann M, Geerts Y, Piris J, Debije MG, van de Craats AM, Senthilkumar K, Siebbeles LDA, Warman JM, Brédas J-L, Cornil J (2004) Charge transport properties in discotic liquid crystals: a

quantum-chemical insight into structure−property relationships. J Am Chem Soc 126(10):3271–3279
24. Brédas J-L, Beljonne D, Coropceanu V, Cornil J (2004) Charge-transfer and energy-transfer processes in π-conjugated oligomers and polymers: a molecular picture. Chem Rev 104(11):4971–5004
25. Valeev EF, Coropceanu V, da Silva Filho DA, Salman S, Brédas J-L (2006) Effect of electronic polarization on charge-transport parameters in molecular organic semiconductors. J Am Chem Soc 128(30):9882–9886
26. Shuai Z, Geng H, Xu W, Liao Y, André JM (2014) From charge transport parameters to charge mobility in organic semiconductors through multiscale simulation. Chem Soc Rev 43:2662–2679
27. Kwon O, Coropceanu V, Gruhn NE, Durivage JC, Laquindanum JG, Katz HE, Cornil J, Brédas JL (2004) Characterization of the molecular parameters determining charge transport in anthradithiophene. J Chem Phys 120(17):8186–8194
28. Tian GJ, Duan S, Hua WJ, Luo Y (2012) DynaVib Version 1.0. Royal Institute of Technology, Sweden
29. Frisch M, Trucks G, Schlegel H, Scuseria G, Robb M, Cheeseman J, Scalmani G, Barone V, Mennucci B, Petersson G, et al Gaussian 09, revision a. 02. Gaussian, Inc., Wallingford, CT
30. Shuai Z, Xu W, Peng Q, Geng H (2013) From electronic excited state theory to the property predictions of the organic optoelectronic materials. Sci China Chem 56(9):1227–1284